Supplementary Inforamation for
Spin orientation switching in oxyfluoride layered perovskite $Pb_3Fe_2O_5F_2$

Kengo Oka,[1] Yusuke Nambu,[2,3,4] Masayuki Ochi,[5] Naoaki Hayashi,[6,7] Yoshihiro Kusano,[8] Takuya Aoyama,[9] Yui Ishii,[10] Kazuhiko Kuroki,[5] Shigeo Mori,[10] Mikio Takano,[7] Naoki Noma,[1] Mitsunobu Iwasaki,[1] and Hiroshi Kageyama[11]

[1]*Department of Applied Chemistry, Faculty of Science and Engineering, Kindai University, Higashi-Osaka, Osaka 577-8502, Japan*
[2]*Institute for Materials Research, Tohoku University, Sendai 980-8577, Japan*
[3]*FOREST, Japan Science and Technology Agency, Kawaguchi, Saitama 332-0012, Japan*
[4]*Organization for Advanced Studies, Tohoku University, Sendai 980-8577, Japan*
[5]*Department of Physics, Osaka University, Toyonaka, Osaka 560-0043, Japan*
[6]*NanoSquare Research Institute, Osaka Prefecture University, Sakai, Osaka 599-8531, Japan*
[7]*Research Institute for Production Development, Kyoto 606-0805, Japan*
[8]*Department of Applied Chemistry and Biotechnology, Okayama University of Science, Okayama, Okayama 700-0005, Japan*
[9]*Department of Physics, Tohoku University, Sendai 980-8578, Japan*
[10]*Department of Materials Science, Osaka Prefecture University, Sakai, Osaka 599-8531, Japan*
[11]*Department of Energy and Hydrocarbon Chemistry, Graduate School of Engineering, Kyoto University, Kyoto 615-8510, Japan*

(Dated: July 1, 2021)

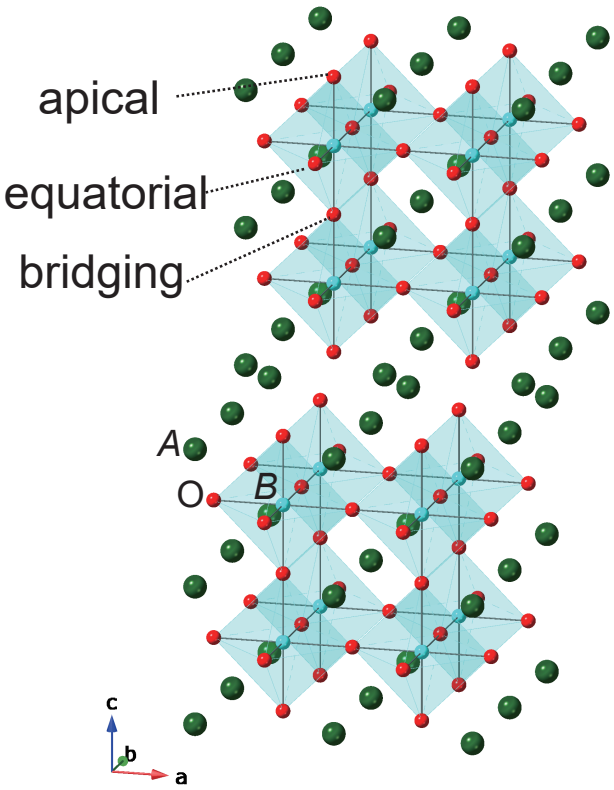

FIG. S1. **Illustration of an ideal Ruddlesden-Popper (RP) type layered perovskite.** The crystal structure for an ideal $A_{n+1}B_nO_{3n+1}$ ($n = 2$) structure. Three distinct anion sites (apical, equatorial, and bridging) are present.

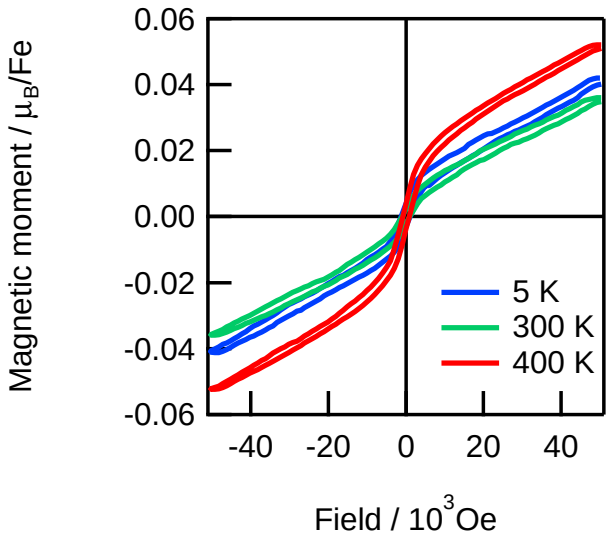

FIG. S2. **Magnetization curves of $Pb_3Fe_2O_5F_2$.** The magnetization curves of $Pb_3Fe_2O_5F_2$ collected at 5, 300, and 400 K. A weak ferromagnetic behavior was observed below the Néel temperature of 490 K.

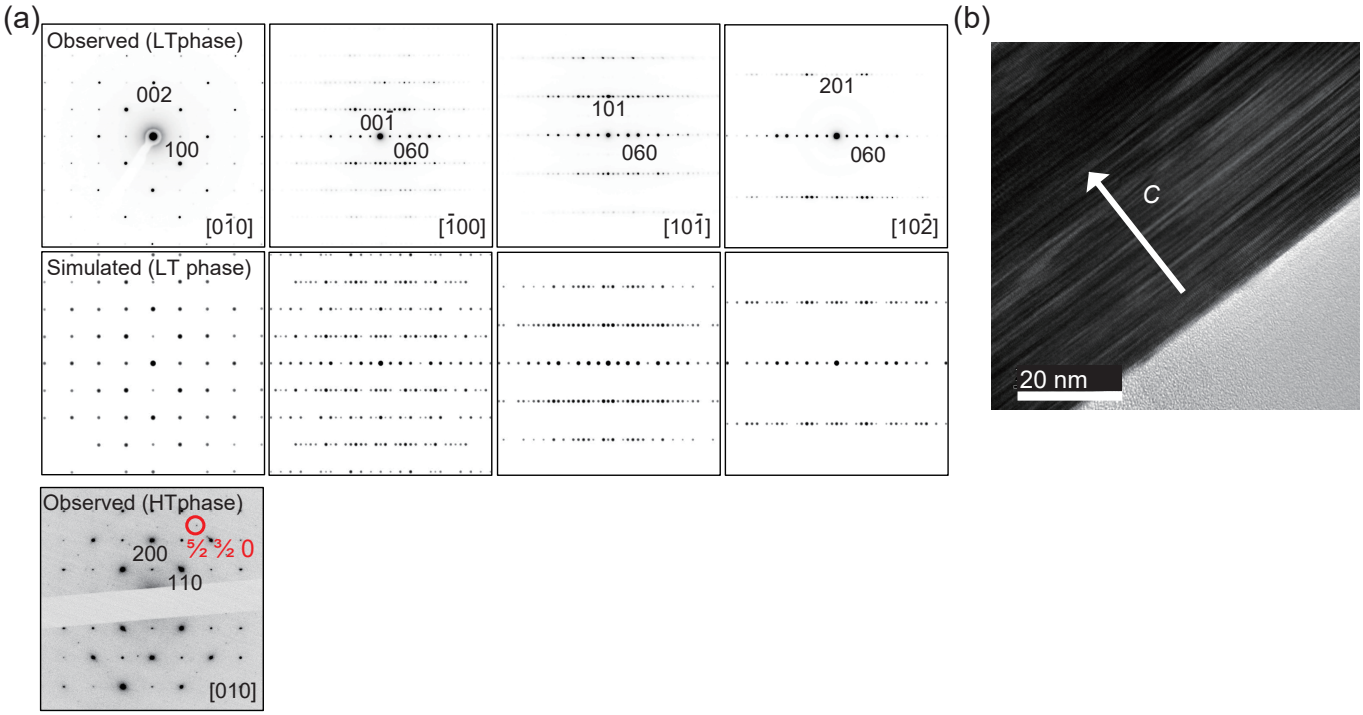

FIG. S3. **TEM study for $Pb_3Fe_2O_5F_2$.** (a) Electron diffraction (ED) patterns collected at room temperature (LT phase) and 500 K (HT phase). The top and middle panels show the observed and simulated patterns using our $P2_1/m$ structure model for the LT phase. The bottom panel is the ED pattern of the HT phase showing appearance of the super structure. (b) TEM image showing stacking fault along the c-axis.

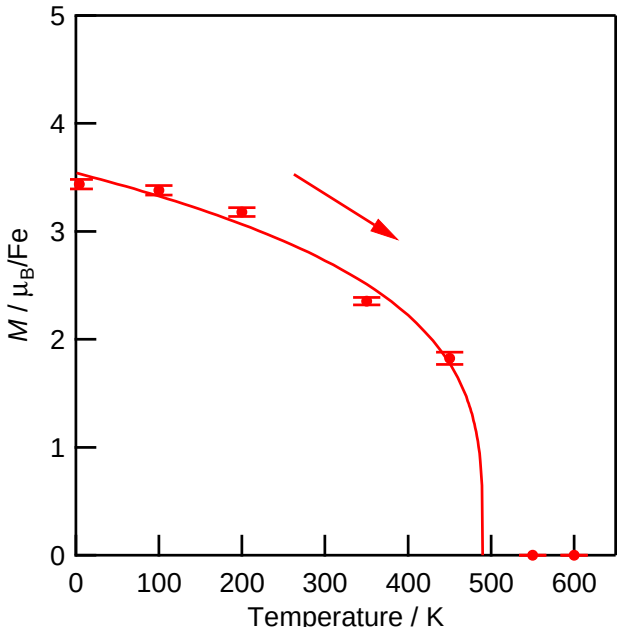

FIG. S4. **Temperature evolution of the refined magnetic moment.** The refined magnetic moment of Fe^{3+} obtained by Rietveld refinement of neutron powder diffraction (NPD) patterns.

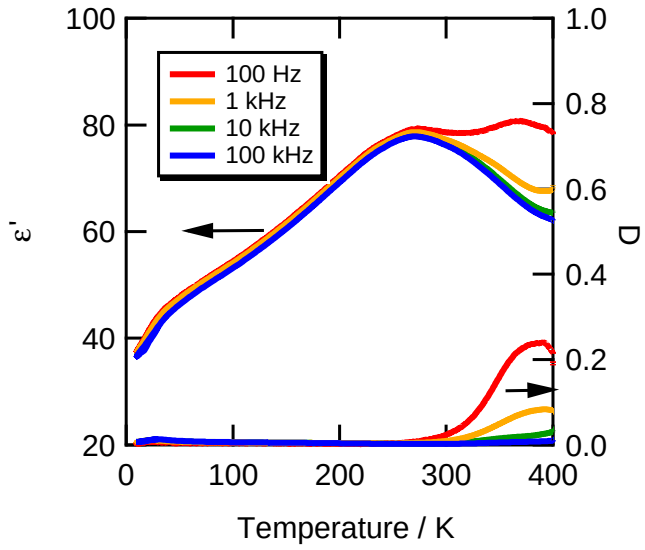

FIG. S5. **Temperature dependence of the dielectric constant (ε') and loss (D) of $Pb_3Fe_2O_5F_2$.** The dielectric loss keeps the magnitude lower than 1 below 400 K, indicating insulating nature.

TABLE I. **The refined ^{57}Fe Mössbauer parameters for $Pb_3Fe_2O_5F_2$.** The abbreviations IS, HF, QS, and FWHM denote isomer shift, hyperfine field, quadrupole splitting, and full width at half maximum, respectively.

Temperature (K)	IS (mm/s)	HF (T)	QS (mm/s)	FWHM (mm/s)	Area ratio
78	0.51	53.5	*-0.32	0.31	1
RT	0.40	43.7	*-0.31	0.31	1
400	0.32	29.5	*-0.34	0.50	1
450	0.28	20.4	*-0.34	0.66	0.86
	0.28	0	0.67	0.60	0.14
500	0.24	0	0.68	0.38	1

* $(S_2 - S_1)/2$. S_1 and S_2 are the separations of the two outer peaks on the lower and higher velocity side of the sextet, respectively. The 'S_1–S_2' of –0.34 mm/s at 400 K in the sextet is nearly half of the magnitude of quadruple splitting (QS) in the paramagnetic state, indicating $\perp z$ spin alignment in the HT phase, where the magnetization vector is perpendicular to the electric filed gradient along the c-axis.

TABLE II. **The refined crystallographic parameters for $Pb_3Fe_2O_5F_2$.** The refined crystallographic parameters were obtained using SXRD patterns at 100 and 550 K.

The LT phase (100 K)						
S.G. $P2_1/m$, $a = 3.94060(5)$ Å, $b = 3.94164(5)$ Å, $c = 21.4002(2)$ Å, $\gamma = 89.8157(8)°$						
Atom	Site	x	y	z	B_{iso}/Å^2	BVS*
Pb1	$4f$	0.2464(7)	0.3445(4)	0.07531(5)	0.30(3)	2.35
Pb2	$2e$	0.2270(9)	0.3297(6)	1/4	0.62(5)	1.94
Fe	$4f$	0.757(2)	0.8711(13)	0.1590(3)	0.46(10)	2.92
O1	$4f$	0.622(9)	0.380(10)	0.1564(17)	6.4(6)	2.03
O2	$4f$	0.216(15)	0.905(9)	0.1384(14)	6.4	2.06
O3	$4f$	0.722(11)	0.949(7)	1/4	0.2(8)	1.88
F	$2e$	0.780(7)	0.861(5)	0.0630(6)	0.2(8)	0.94
The HT phase (550 K)						
S.G.: $P4_2/nbc$, $a = 7.89769(2)$ Å, $c = 21.8851(1)$ Å						
Atom	Site	x	y	z	B_{iso}/Å^2	BVS*
Pb1	$8i$	-0.0006(15)	1/4	1/2	3.16(3)	1.95
Pb2	$16k$	0.0008	0.7485(7)	0.32776(3)	1.92(2)	2.01
Fe	$16k$	-0.0013(19)	0.7566(18)	0.91121(12)	1.18(6)	2.75
O1	$8h$	0.064(3)	1/4	0	2.0(4)	1.91
O2	$8f$	1/4	1/4	0.1167	1.6(4)	2.13
O3	$8g$	3/4	1/4	0.097(3)	1.6	1.88
O4	$16k$	-0.013(6)	0.049(3)	0.4086(14)	1.6	1.97
F	$16k$	-0.008(7)	0.751(7)	0.8109(4)	2.0	0.80

* Bond valence sums (BVS) were calculated assuming complete O/F order.

MAGNETIC STRUCTURE ANALYSIS

We employed group theoretical analysis based upon irreducible representation to identify the magnetic structure for both high- and low-temperature phases. For the high-temperature phase at $T = 400$ K, all magnetic peak positions can be indexed by a propagation wave vector, $\boldsymbol{q}_{\rm m}^{\rm high} = (0, 0, 0)$. Basis vectors (BVs) of the irreducible representations (irreps) for the wave vector are summarised in Table III.

There are 10 irreps in total, and each irrep consists of 3–12 BVs giving relations of magnetic moment directions. First, we sorted out all BVs by comparing magnetic R-factor and found ψ_{14} in Γ_5 has the best fit with $R_{\rm mag} = 19.8$ %. The second best refinement was achieved by ψ_7 in Γ_3 with 20.5 %, and the others poorly describe our data ($R_{\rm mag} >$ 25 %). The magnetic transition in the high-temperature phase is of second order, allowing the adoption of multiple BVs within the same irrep to describe the magnetic structure. We then tested the potential involving of BVs for all the irreps including Γ_3, however, they cannot improve fitting quality. The magnetic structure with ψ_{14} is depicted in Fig. 4b in the main text.

For the low-temperature phase at $T = 4$ K, additional peaks are found, and they can be indexed by a propagation wave vector, $\boldsymbol{q}_{\rm m}^{\rm low} = (1/2, 0, -1/2)$ in the $P2_1/m$ space group. Table IV summarises BVs of the irreps for the wave vector $\boldsymbol{q}_{\rm m}^{\rm low}$.

There are allowed 4 irreps, and each irrep consists of 3 BVs. We likewise sorted out all BVs by comparing magnetic R-factor and found ψ_5 in Γ_2 has the best fit with $R_{\rm mag} = 16.8$ %. The second best refinement was by ψ_8 in Γ_3 (16.9 %). These results from ψ_5 and ψ_8 are actually very close, and the difference is only found in the stacking sequence along the b-axis. Since the low-temperature phase is after the first order transition, the magnetic structure could be described by arbitrary combinations of BVs. We tested all of them, and found that either ψ_5 or ψ_8 plus the participation of small moments within the ac-plane would improve the fitting quality. However, refinements of tiny moments based upon powder data are very difficult, and the resultant magnetic structure can be approximated as the G-type with the moments along the b-axis. Future refinements with a single crystalline sample would be able to evaluate tiny ac-moments. For the low-temperature phase, the magnetic structure with ψ_5 is depicted in Fig. 4d in the main text.

FIRST PRINCIPLES CALCULATION

We used the Perdew-Burke-Ernzerhof parametrization of the generalized gradient approximation [1] and the projector augmented wave method [2] as implemented in the Vienna Ab initio Simulation Package [3–6]. The crystal structure parameters listed on Supplementary Table 2 were used in our calculation. The plane-wave cutoff energy of 450 eV was used. We used $14 \times 14 \times 3$, $16 \times 16 \times 4$, $8 \times 8 \times 3$, $10 \times 10 \times 4$ **k**-meshes for the self-consistent-field calculation of LT structure, DOS calculation of LT structure, those for HT structure, respectively. The G-type antiferromagnetic order was assumed. Since we perturbatively interpreted the spin-orbit coupling for understanding the magnetic anisotropy, the energy levels used in our discussion as the non-perturbative states were calculated without including the spin-orbit coupling.

[1] J. P. Perdew, K. Burke, and M. Ernzerhof, Phys. Rev. Lett. **77**, 3865 (1996).
[2] G. Kresse and D. Joubert, Phys. Rev. B **59**, 1758 (1999).
[3] G. Kresse and J. Hafner, Phys. Rev. B **47**, 558(R) (1993).
[4] G. Kresse and J. Hafner, Phys. Rev. B **49**, 14251 (1994).
[5] G. Kresse and J. Furthmuller, Comput. Mater. Sci. **6**, 15 (1996).
[6] G. Kresse and J. Furthmuller, Phys. Rev. B **54**, 11169 (1996).

TABLE III. Basis vectors (BVs) of irreducible representations (irreps) for the space group $P4_2/nbc$ with the magnetic wave vector $\boldsymbol{q}_{\rm m} = (0, 0, 0)$. Superscirpts show the moment direction. Columns for positions represent #1: $(x = .00073, y = .75159, z = .91082)$, #2: $(x, -y + 1/2, -z)$, #3: $(-x + 1/2, y, -z)$, #4: $(-x + 1/2, -y + 1/2, z)$, #5: $(-y + 1/2, -x + 1/2, -z + 1/2)$, #6: $(-y + 1/2, x, z + 1/2)$, #7: $(y, -x + 1/2, z + 1/2)$, #8: $(y, x, -z + 1/2)$, #9: $(-x, -y, -z)$, #10: $(-x, y + 1/2, z)$, #11: $(x + 1/2, -y, z)$, #12: $(x + 1/2, y + 1/2, -z)$, #13: $(y + 1/2, x + 1/2, z + 1/2)$, #14: $(y + 1/2, -x, -z + 1/2)$, #15: $(-y, x + 1/2, -z + 1/2)$, and #16: $(-y, -x, z + 1/2)$.

irrep	BV	#1	#2	#3	#4	#5	#6	#7	#8	#9	#10	#11	#12	#13	#14	#15	#16
	ψ_1	1^a	1^a	-1^a	-1^a	-1^b	1^b	-1^b	1^b	1^a	1^a	-1^a	-1^a	-1^b	1^b	-1^b	1^b
Γ_1	ψ_2	1^b	-1^b	1^b	-1^b	-1^a	-1^a	1^a	1^a	1^b	-1^b	1^b	-1^b	-1^a	-1^a	1^a	1^a
	ψ_3	1^c	-1^c	-1^c	1^c	-1^c	1^c	1^c	-1^c	1^c	-1^c	-1^c	1^c	-1^c	1^c	1^c	-1^c
	ψ_4	1^a	1^a	-1^a	-1^a	-1^b	1^b	-1^b	1^b	-1^a	-1^a	1^a	1^a	1^b	-1^b	1^b	-1^b
Γ_2	ψ_5	1^b	-1^b	1^b	-1^b	-1^a	-1^a	1^a	1^a	-1^b	1^b	-1^b	1^b	1^a	1^a	-1^a	-1^a
	ψ_6	1^c	-1^c	-1^c	1^c	-1^c	1^c	1^c	-1^c	-1^c	1^c	1^c	-1^c	1^c	-1^c	-1^c	1^c
	ψ_7	1^a	-1^a	1^a	-1^a	1^b	1^b	-1^b	-1^b	1^a	-1^a	1^a	-1^a	1^b	1^b	-1^b	-1^b
Γ_3	ψ_8	1^b	1^b	-1^b	-1^b	1^a	-1^a	1^a	-1^a	1^b	1^b	-1^b	-1^b	1^a	-1^a	1^a	-1^a
	ψ_9	1^c	1^c	1^c	1^c	1^c	1^c	1^c	1^c	1^c	1^c	1^c	1^c	1^c	1^c	1^c	1^c
	ψ_{10}	1^a	-1^a	1^a	-1^a	1^b	1^b	-1^b	-1^b	-1^a	1^a	-1^a	1^a	-1^b	-1^b	1^b	1^b
Γ_4	ψ_{11}	1^b	1^b	-1^b	-1^b	1^a	-1^a	1^a	-1^a	-1^b	-1^b	1^b	1^b	-1^a	1^a	-1^a	1^a
	ψ_{12}	1^c	1^c	1^c	1^c	1^c	1^c	1^c	1^c	-1^c	-1^c	-1^c	-1^c	-1^c	-1^c	-1^c	-1^c
	ψ_{13}	1^a	1^a	-1^a	-1^a	1^b	-1^b	1^b	-1^b	1^a	1^a	-1^a	-1^a	1^b	-1^b	1^b	-1^b
Γ_5	ψ_{14}	1^b	-1^b	1^b	-1^b	1^a	1^a	-1^a	-1^a	1^b	-1^b	1^b	-1^b	1^a	1^a	-1^a	-1^a
	ψ_{15}	1^c	-1^c	-1^c	1^c	1^c	-1^c	-1^c	1^c	1^c	-1^c	-1^c	1^c	1^c	-1^c	-1^c	1^c
	ψ_{16}	1^a	1^a	-1^a	-1^a	1^b	-1^b	1^b	-1^b	-1^a	-1^a	1^a	1^a	-1^b	1^b	-1^b	1^b
Γ_6	ψ_{17}	1^b	-1^b	1^b	-1^b	1^a	1^a	-1^a	-1^a	-1^b	1^b	-1^b	1^b	-1^a	-1^a	1^a	1^a
	ψ_{18}	1^c	-1^c	-1^c	1^c	1^c	-1^c	-1^c	1^c	-1^c	1^c	1^c	-1^c	-1^c	1^c	1^c	-1^c
	ψ_{19}	1^a	-1^a	1^a	-1^a	-1^b	-1^b	1^b	1^b	1^a	-1^a	1^a	-1^a	-1^b	-1^b	1^b	1^b
Γ_7	ψ_{20}	1^b	1^b	-1^b	-1^b	-1^a	1^a	-1^a	1^a	1^b	1^b	-1^b	-1^b	-1^a	1^a	-1^a	1^a
	ψ_{21}	1^c	1^c	1^c	1^c	-1^c	-1^c	-1^c	-1^c	1^c	1^c	1^c	1^c	-1^c	-1^c	-1^c	-1^c
	ψ_{22}	1^a	-1^a	1^a	-1^a	-1^b	-1^b	1^b	1^b	-1^a	1^a	-1^a	1^a	1^b	1^b	-1^b	-1^b
Γ_8	ψ_{23}	1^b	1^b	-1^b	-1^b	-1^a	1^a	-1^a	1^a	-1^b	-1^b	1^b	1^b	1^a	-1^a	1^a	-1^a
	ψ_{24}	1^c	1^c	1^c	1^c	-1^c	-1^c	-1^c	-1^c	-1^c	-1^c	-1^c	-1^c	1^c	1^c	1^c	1^c
	ψ_{25}	1^a	1^a	1^a	1^a	0	0	0	0	1^a	1^a	1^a	1^a	0	0	0	0
	ψ_{26}	1^b	-1^b	-1^b	1^b	0	0	0	0	1^b	-1^b	-1^b	1^b	0	0	0	0
	ψ_{27}	1^c	-1^c	1^c	-1^c	0	0	0	0	1^c	-1^c	1^c	-1^c	0	0	0	0
	ψ_{28}	0	0	0	0	-1^b	1^b	1^b	-1^b	0	0	0	0	-1^b	1^b	1^b	-1^b
	ψ_{29}	0	0	0	0	-1^a	-1^a	-1^a	-1^a	0	0	0	0	-1^a	-1^a	-1^a	-1^a
Γ_9	ψ_{30}	0	0	0	0	-1^c	1^c	-1^c	1^c	0	0	0	0	-1^c	1^c	-1^c	1^c
	ψ_{31}	0	0	0	0	-1^b	-1^b	-1^b	-1^b	0	0	0	0	-1^b	-1^b	-1^b	-1^b
	ψ_{32}	0	0	0	0	-1^a	1^a	1^a	-1^a	0	0	0	0	-1^a	1^a	1^a	-1^a
	ψ_{33}	0	0	0	0	-1^c	-1^c	1^c	1^c	0	0	0	0	-1^c	-1^c	1^c	1^c
	ψ_{34}	1^a	-1^a	-1^a	1^a	0	0	0	0	1^a	-1^a	-1^a	1^a	0	0	0	0
	ψ_{35}	1^b	1^b	1^b	1^b	0	0	0	0	1^b	1^b	1^b	1^b	0	0	0	0
	ψ_{36}	1^c	1^c	-1^c	-1^c	0	0	0	0	1^c	1^c	-1^c	-1^c	0	0	0	0
	ψ_{37}	1^a	1^a	1^a	1^a	0	0	0	0	-1^a	-1^a	-1^a	-1^a	0	0	0	0
	ψ_{38}	1^b	-1^b	-1^b	1^b	0	0	0	0	-1^b	1^b	1^b	-1^b	0	0	0	0
	ψ_{39}	1^c	-1^c	1^c	-1^c	0	0	0	0	-1^c	1^c	-1^c	1^c	0	0	0	0
	ψ_{40}	0	0	0	0	-1^b	1^b	1^b	-1^b	0	0	0	0	1^b	-1^b	-1^b	1^b
	ψ_{41}	0	0	0	0	-1^a	-1^a	-1^a	-1^a	0	0	0	0	1^a	1^a	1^a	1^a
Γ_{10}	ψ_{42}	0	0	0	0	-1^c	1^c	-1^c	1^c	0	0	0	0	1^c	-1^c	1^c	-1^c
	ψ_{43}	0	0	0	0	-1^b	-1^b	-1^b	-1^b	0	0	0	0	1^b	1^b	1^b	1^b
	ψ_{44}	0	0	0	0	-1^a	1^a	1^a	-1^a	0	0	0	0	1^a	-1^a	-1^a	1^a
	ψ_{45}	0	0	0	0	-1^c	-1^c	1^c	1^c	0	0	0	0	1^c	1^c	-1^c	-1^c
	ψ_{46}	1^a	-1^a	-1^a	1^a	0	0	0	0	-1^a	1^a	1^a	-1^a	0	0	0	0
	ψ_{47}	1^b	1^b	1^b	1^b	0	0	0	0	-1^b	-1^b	-1^b	-1^b	0	0	0	0
	ψ_{48}	1^c	1^c	-1^c	-1^c	0	0	0	0	-1^c	-1^c	1^c	1^c	0	0	0	0

TABLE IV. Basis vectors (BVs) of irreducible representations (irreps) for the space group $P2_1/m$ with the magnetic wave vector $\boldsymbol{q}_{\rm m} = (1/2, 0, -1/2)$. Columns for positions represent #1: $(x = .87682, y = .15942, z = .74759)$, #2: $(-x, y + 1/2, -z)$, #3: $(-x, -y, -z)$, and #4: $(x, -y + 1/2, z)$.

irrep	BV	#1	#2	#3	#4
Γ_1	ψ_1 ($\parallel a$)	1	-1	1	-1
	ψ_2 ($\parallel b$)	1	1	1	1
	ψ_3 ($\parallel c$)	1	-1	1	-1
Γ_2	ψ_4 ($\parallel a$)	1	-1	-1	1
	ψ_5 ($\parallel b$)	1	1	-1	-1
	ψ_6 ($\parallel c$)	1	-1	-1	1
Γ_3	ψ_7 ($\parallel a$)	1	1	1	1
	ψ_8 ($\parallel b$)	1	-1	1	-1
	ψ_9 ($\parallel c$)	1	1	1	1
Γ_4	ψ_{10} ($\parallel a$)	1	1	-1	-1
	ψ_{11} ($\parallel b$)	1	-1	-1	1
	ψ_{12} ($\parallel c$)	1	1	-1	-1